

Porous Low-Loss Silica–PMMA Dielectric Nanocomposite for High-Frequency Bullet Lens Applications

Petra S. Palvölgyi, Mikko Kokkonen, Rafal Sliz, Heli Jantunen, Krisztian Kordas, and Sami Myllymäki*

Several devices of the future generation wireless telecommunication technologies that use bands in THz frequencies for data transmission need low-loss and low-permittivity materials to enable ideal conditions for the propagation of electromagnetic waves. Herein, a lightweight dielectric bullet-shaped lens operating in the frequency range of 110–170 GHz is demonstrated to collimate electromagnetic waves, thus increasing the intensity of the electric field. The material of the lens is based on a composite of silica nanoshells and poly(methylmethacrylate) made by the impregnation of the nanoshells with the polymer followed by hot pressing in a mold. As the polymer acts only as an adhesive between the hollow nanospheres without filling the inner cavity of the shells and their interparticle spaces, the composite is highly porous (67%) and has low dielectric permittivity and loss tangent (1.5 and 4×10^{-3} , respectively, below 200 GHz). The size of the collimated beam and the increase of the corresponding field strength are measured to vary from 2.2 to 1.2 mm and from 17.2 to 8.98 dB depending on the frequency of the waves (110–170 GHz).

1. Introduction

Of the sixth generation (6G) telecommunication technologies, Internet of Things (IoT) is one of the most attractive features that allows fully automated human-free control and operation of connected devices, to create smart homes, institutes, factories, transportation, and cities. IoT may be assisted by artificial intelligence (AI) to increase the efficiency of the networks by providing complex problem-solving ability. Applications, which need real-time

data processing, will be allowed by mobility-enhanced edge computing (MEEC) which is the modified version of cloud computing, bringing services closer to the end user, having quicker response time. The operation of battery-less smart devices will be ensured by wireless information and energy transfer (WIET) and unmanned aerial vehicles (UAV)/drones will be integrated into 6G to provide cellular connectivity and high data rate. Clearly, the implementation of these technologies requires enormous number of devices communicating wirelessly, thus high data transfer rate needs to be guaranteed. As the currently used frequency bands cannot transfer the amount of data demanded by these technologies, moving to bands of shorter wavelengths (0.1–10 THz) will increase the capacity by 1000 times in 6G in comparison to the fifth generation


(5G) wireless telecommunication technology. Furthermore, applications with real-time response demand improved reliability (99.9%) and high data transmission rate ($\approx 1 \text{ TB s}^{-1}$) with ultra-low latency (1 ms), as expected in 6G.^[1–5]

As the path loss of electromagnetic (EM) waves increases with the frequency, antennas operating at THz frequency band need to have especially high gain and/or shall be equipped with lenses to ensure sufficiently high intensities. The operation of lenses is based on either diffraction (e.g., zone plate lenses)^[6,7] or refraction of the EM waves. Of the latter, we may distinguish heterogeneous and homogeneous lenses depending on whether the refraction of the waves occurs within the bulk or on the surface of the dielectric lens.^[8,9] Regardless of the type of the lens, the material it is made of is expected to have low loss ($\tan \delta$) to avoid signal attenuation.^[10] Lens materials of high permittivity (ϵ_r) allow for relatively thin lens designs with small surface curvatures but necessitate the use of gradient structures in the proximity of the surface to minimize reflection losses. The production of such gradient structures is not trivial, thus making heterogeneous lenses less attractive than their homogeneous counterparts based on low-permittivity materials.^[11]

Among dielectrics, silica has good electromagnetic properties ($\epsilon_r = 3.8$ and $\tan \delta = 0.005$ at 300 GHz) and thus it is a popular choice of structural materials in high-frequency applications. Lowering ϵ_r and $\tan \delta$ of SiO_2 can be achieved by 1) partially replacing easy-to-polarize Si–O bonds with Si–F bonds (e.g., by F doping);^[12,13] 2) introducing voids (e.g., pores filled

P. S. Palvölgyi, M. Kokkonen, H. Jantunen, K. Kordas, S. Myllymäki
Microelectronics Research Unit
Faculty of Information and Electrical Engineering
University of Oulu
P. O. Box 4500, FI-90570 Oulu, Finland
E-mail: sami.myllymaki@oulu.fi

R. Sliz
Optoelectronics and Measurement Techniques Unit
Faculty of Information Technology and Electrical Engineering
University of Oulu
P.O. Box 4500, FI-90014 Oulu, Finland

 The ORCID identification number(s) for the author(s) of this article can be found under <https://doi.org/10.1002/adpr.202200208>.

© 2023 The Authors. Advanced Photonics Research published by Wiley-VCH GmbH. This is an open access article under the terms of the Creative Commons Attribution License, which permits use, distribution and reproduction in any medium, provided the original work is properly cited.

DOI: 10.1002/adpr.202200208

Table 1. Different silica-based materials and their relative dielectric permittivity.

Material	Synthesis method	ϵ_r	References
Silica	–	3.9–4.5	[12]
Fluorosilicate glass	F-doping	3.6–3.8	[12]
Fluorosilicate glass	F-doping	2.8	[13]
Porous silica	Template-assisted synthesis	1.9	[14]
Porous silica	CVD and thermal decomposition	2.2	[15]
Fluorinated silica–PI composite	Chemical decomposition and grafting	2.6	[16]
Silica–PI composite	Template-assisted synthesis and thermal polymerization	2.1	[17]
Porous silica–PMMA composite	Template-assisted synthesis and thermal polymerization	2.7	[18]
PTFE–silica composite	Sintering	1.9	[19]

with air);^[14,15] and/or 3) combining volumes of other phases having low permittivity (e.g., compounding SiO₂ with polymers)^[16–19] (Table 1).

In this work, we build on the latter two strategies by applying hollow silica nanospheres (i.e., nanoshells) that we physically bind together with a low-permittivity and low-loss ($\epsilon_r = 2.67$ and $\tan \delta = 0.027$ at 500 GHz)^[20] poly(methylmethacrylate) phase having a small volume fraction in the composite without forming a continuous matrix in the interparticle space. With this effort, not only the low permittivity and loss are ensured but also the mechanical integrity and option for postprocessing of the composite are achieved. To demonstrate the feasibility of the as-made material for high-frequency applications, the composite is hot-pressed in a mold to form a bullet-shaped lens operating at a central frequency of 140 GHz.

2. Experimental Section

2.1. Materials

Polyvinylpyrrolidone ($M = 10\,000\text{ g mol}^{-1}$), styrene, potassium persulfate, hexadecyltrimethylammonium bromide ($\geq 99\%$), ammonium hydroxide solution (25 wt%), tetraethyl orthosilicate ($\geq 99\%$), 2-(2-butoxyethoxy)ethyl acetate, PMMA ($M = 350\,000\text{ g mol}^{-1}$), and absolute ethanol (99.5 wt%) were purchased from Sigma–Aldrich and Altia, respectively, and used as received without further purification.

2.2. Synthesis of Silica Nanoshells

Hollow silica nanoshells were synthesized by template-assisted Stöber process, similar to that as reported earlier.^[21] In short, first, polymer template spheres were synthesized by emulsion polymerization of styrene monomers using potassium persulfate as initiator. Next, the polymer spheres were covered with a thin layer of silica by polycondensation of tetraethyl orthosilicate in the presence of ammonium hydroxide. Finally, the polymer core of the coated particles was burned out resulting in the silica nanoshell product.

2.3. Preparation of the Porous Silica–PMMA Composite

Microspheres of PMMA were dissolved in 2-(2-butoxyethoxy) ethyl acetate (14 wt%), by stirring the mixture at 90 °C for 3 h, and

the solution was cooled down to room temperature. In the next step, silica nanoshells were mixed with acetone in 1:1 volume ratio and added to the polymer solution to obtain a mixture with a composition of $V_{\text{silica shells}}:V_{\text{acetone}}:V_{\text{PMMA solution}} = 1:1:0.7$. This mixture was then poured into the cavity of a polyvinylidene-fluoride ring (12 mm in inner diameter and 2 mm in thickness) placed on a plate, which served as a mold for a producing a slab of the composite. The filled ring was then covered with a perforated release foil (silicon-coated polyethylene terephthalate film), a wipe (nonwoven polyester/cellulose), and then with a glass slide. The structure was placed in a box oven, to evaporate the solvents (50 °C for 2 h followed by 110 °C for overnight). After drying, a small aliquot (100–150 μL) of additional PMMA solution was dropped on the slabs and dried at 110 °C for ≈ 12 h, which was repeated 8 times to provide sufficient amount of PMMA that binds the nanoshells together. The final composition of the composite was calculated to be 79.8 wt% PMMA and 20.2 wt% silica

2.4. Preparation of PMMA Reference Samples for Dielectric Measurements

PMMA reference samples were obtained by pouring 14 wt% polymer solution into a mold, similar to that of used for the composite preparation and placed into a box oven for overnight at 110 °C to evaporate the solvent. Droplets of the polymer solution were added onto the slabs followed by evaporation, until the solid polymer filled the mold, completely.

2.5. Hot Pressing of the Dielectric Lens

To prepare the dielectric lens (Figure 1), 0.312 g of silica–PMMA composite was broken into small (≈ 0.5 mm) pieces by a spatula and mixed with 0.2 mL of 2-(2-butoxyethoxy)ethyl acetate. The mixture was then transferred into a two-piece bullet-shaped mold and pressed (P/O/WEBER PW 20 HS Hotpress, 5 kPa, 200 °C, 10 min). After releasing the pressure and cooling, the sample was placed in an oven to dry completely at 200 °C for overnight.

3. Characterization

Field emission scanning electron microscopy (FESEM, Zeiss Ultra Plus) and transmission electron microscopy (TEM Jeol

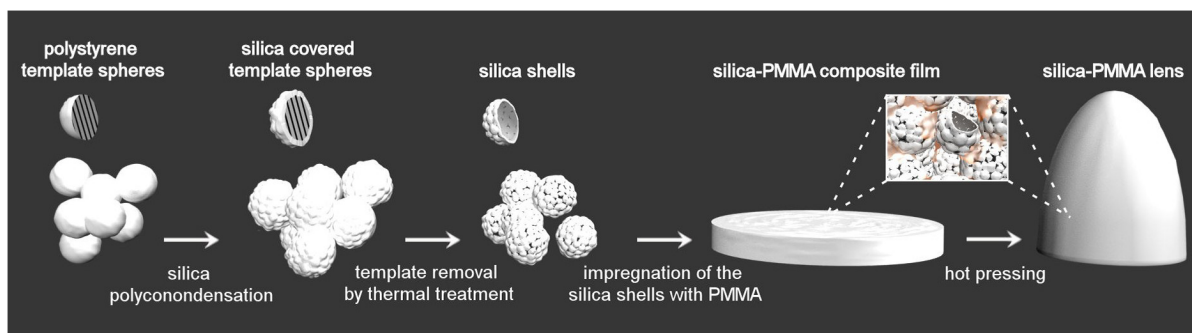


Figure 1. Schematic sequence of bullet-shaped lens fabrication.

Jem-2200FS) were used to analyze the morphology and microstructure of the synthesized materials. To determine the size distribution of the obtained polymer template spheres, silica-coated polymer spheres, and hollow silica nanoshells, Fiji ImageJ software was used to analyze FESEM and TEM images of 100 particles of each. From dimension and weight measurements, the density and porosity of the composite slabs were calculated. The surface of the hot-pressed dielectric lens was characterized with an optical profilometer (Bruker Contour GT-K) to evaluate the surface roughness (root mean square height).

Dielectric properties of the PMMA reference and silica-PMMA composite slabs were determined by THz spectroscopy (TeraPulse 4000) at frequency range of 0.1–1.5 THz, measuring air at the beginning for reference (90 dB dynamic range at the peak, 100 ps optical delay extent, 200 ps s⁻¹ sweep speed, 50-fold averaging, high-resolution mode with 10 ps prescan extent). The real and imaginary parts of dielectric permittivity were calculated from the Fourier transformed amplitude-time data transmitted through the samples. The beam was limited by a metallic

aperture of 11 mm in diameter. The effective permittivity of the porous composites was calculated by Maxwell-Garnett effective medium approximation model^[22]

$$\epsilon_{MG} = \epsilon_h \frac{\epsilon_i + \frac{1+2f}{3}(\epsilon_i - \epsilon_h)}{\epsilon_h + \frac{1-f}{3}(\epsilon_i - \epsilon_h)} \quad (1)$$

where ϵ_{MG} is the effective permittivity, ϵ_h is the relative permittivity of the host medium, ϵ_i is the relative permittivity of inclusions, and f is the volume filling factor. The bullet-shaped porous composite lens was mounted on a 3-axes transfer stage between two fixed frequency extenders (WR 6.5 (110–170 GHz), Virginia diodes, USA) and characterized using a network analyzer (N5242B PNA-X, Keysight, USA).

4. Results and Discussion

The spherical polystyrene templates (Figure 2a) synthesized by emulsion polymerization have an average diameter of

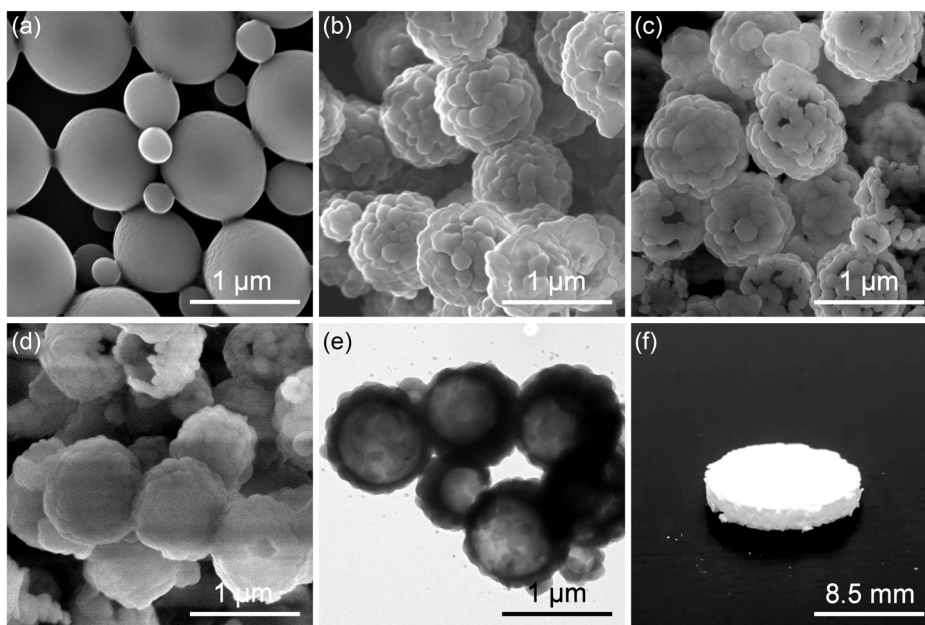


Figure 2. FESEM images of a) polystyrene template spheres, b) silica covered template spheres, c) hollow silica spheres, and d) silica-PMMA composite. e) TEM and f) camera images of the silica-PMMA composite.

937 ± 284 nm. After the polycondensation reaction, the polymer spheres are covered with a thin silica layer, creating a core–shell structure with raspberry-like porous surface (Figure 2b) having an average diameter of 988 ± 62 nm. After the organic core is burned off at 550 °C, hollow porous silica spheres (Figure 2c) with average diameter of 880 ± 141 nm are obtained. To prepare dielectric films (Figure 2f) with sufficient mechanical stability, hollow silica nanospheres are mixed with acetone and dissolved PMMA, the mixture is poured into a mold, let dry at elevated temperature, and got additional droplets of PMMA solution to obtain a composition of 79.8 wt% PMMA and 20.2 wt% silica, having diameter and thickness of 12.0 and 1.7 mm, respectively. According to electron microscopy analysis (Figure 2d,e), the inner cavity of the hollow silica spheres remained to be unfilled with the polymer. In addition, the interparticle space is found to be mostly empty, i.e., the polymer phase of the composite acts only as a thin adhesive between the nanoshells, which explains the measured low density (0.44 g cm⁻³) and high porosity (67%) of the composite.

The dielectric properties of silica–PMMA composite and PMMA polymer reference slabs are measured at frequency range of 0.1–1.5 THz using THz spectroscopy (Figure 3). The composite has low relative part of permittivity, $\epsilon_r' \approx 1.5$ at the whole measured frequency range, in good agreement with the calculated effective permittivity (1.4). The loss factor, $\tan\delta$, is 4.0×10^{-3} at 140 GHz and increases with the frequency as it is expected. The improvements of dielectric properties of silica–PMMA samples compared to those of PMMA slabs are reasonable,

considering the porosity of the composite samples. The lower $\tan\delta$ of the composite is also a result of the presence of silica, having smaller loss than that of the polymer.

Although additional PMMA added to the composite would enhance the mechanical strength, it would result in porosity reduction and consequently increased dielectric permittivity. As calculated by the Maxwell–Garnett approximation, an increased concentration of PMMA by 5 and 10 wt% would decrease the porosity by 14% and 33%, resulting in higher effective permittivity values of 1.7 and 1.9, respectively.

As PMMA is a thermoplastic, it is anticipated that the silica–PMMA composite is feasible for further processing using molding, hot pressing, or other similar methods to create lens with, e.g., bullet shape. At mm-wave frequency bands, different commercial and noncommercial lens materials are applied such as polystyrene, polymethacrylate, acrylonitrile butadiene styrene, or polyetherimide, developed by different ways, having various dielectric properties (Table 2). The dielectric properties, fabrication complexity, and size of porous silica–PMMA composite lens are better or comparable than those listed in Table 2.

To form bullet-shaped lens, we crashed the composite slabs into grains of $\approx 500 \mu\text{m}$ size and fused those again by hot pressing in a mold (Figure 4a). Dimension and weight measurements revealed that the hot pressing process had no effect on the porosity of the composite. The surface roughness (root mean square height) of the hot-pressed lens is $\approx 4.8 \mu\text{m}$, according to measurement carried out by an optical profilometer (Figure 4b).

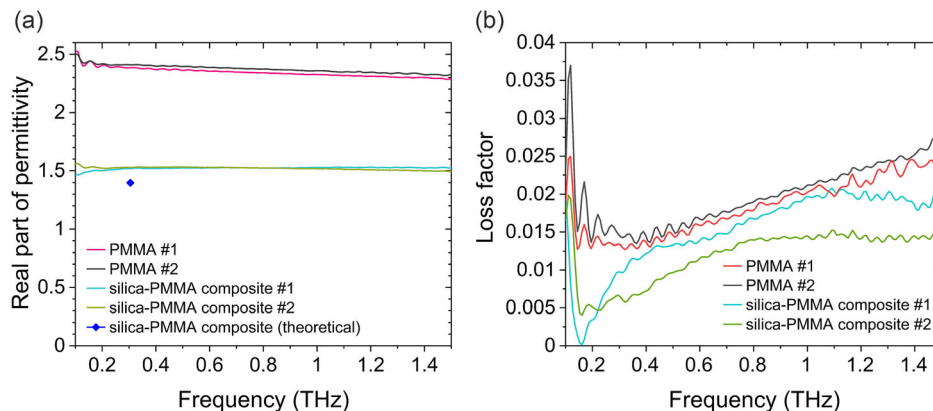


Figure 3. a) Measured and calculated real part of dielectric permittivity and b) measured loss tangent of PMMA and silica–PMMA composite samples.

Table 2. Comparison of silica–PMMA composite with other lens materials, applied at mm-waves (PS, PMA, ABS, and PEI correspond to polystyrene, polymethacrylate, acrylonitrile butadiene styrene, and polyetherimide, respectively).

Lens material	ϵ_r	$\tan\delta$	Lens structure	Fabrication process	Fabrication complexity	Size	Operation frequency [GHz]	References
PS (commercial)	2.53	n.a.	Extended hemisphere	CNC micromachining	Low	27 mm × 25 mm	290	[36]
PMA (commercial)	2.85	2.9×10^{-2}	Hemisphere	3D printing	Low	3 mm × 3 mm	225	[37]
ABS	≈ 2.85	$\approx 1.7 \times 10^{-2}$	Hemisphere	3D printing	Low	9 mm × 9.5 mm	235	[38,39]
PEI	1.12–2.3	7×10^{-3} – 1.6×10^{-2}	Planar zone plate	Foam press	High	120 mm × 2.5 mm	92	[40]
Silica–PMMA composite	1.5	4×10^{-3}	Bullet-shaped	Hot-pressed	Low	9.9 mm × 10.5 mm	140	This work

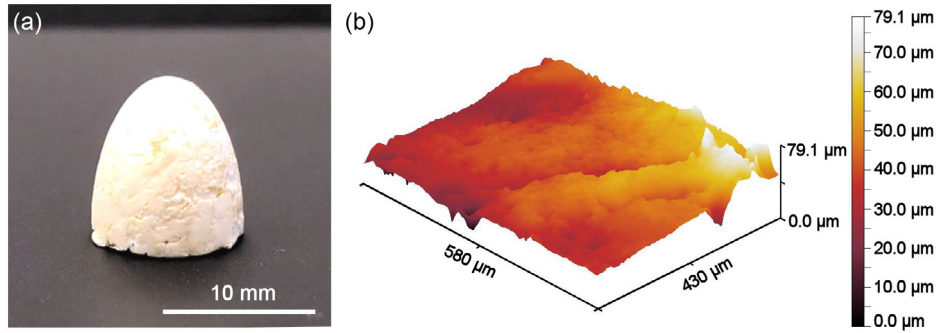


Figure 4. a) Camera image of porous silica–PMMA lens. b) Surface profile of the lens at the top side.

To assess the focusing behavior of the lens, the scattering parameter (S_{21}) of the transmitted beam was measured. The lens was placed on a 3-axis transfer stage, in the optimal position at the optical path (x direction) between the fixed transmitter and receiver, and was moved in y and z directions by 0.25 mm steps

to map an area of 8×7 mm of radiative field as shown in **Figure 5a**. The shape and the size of the measured focal spot slightly changed with frequency (Figure 5b,c). At 110 GHz, the spot is oval and has two sidelobes in the harmonic pattern, whereas at 140 and 170 GHz the focal spots are round and have

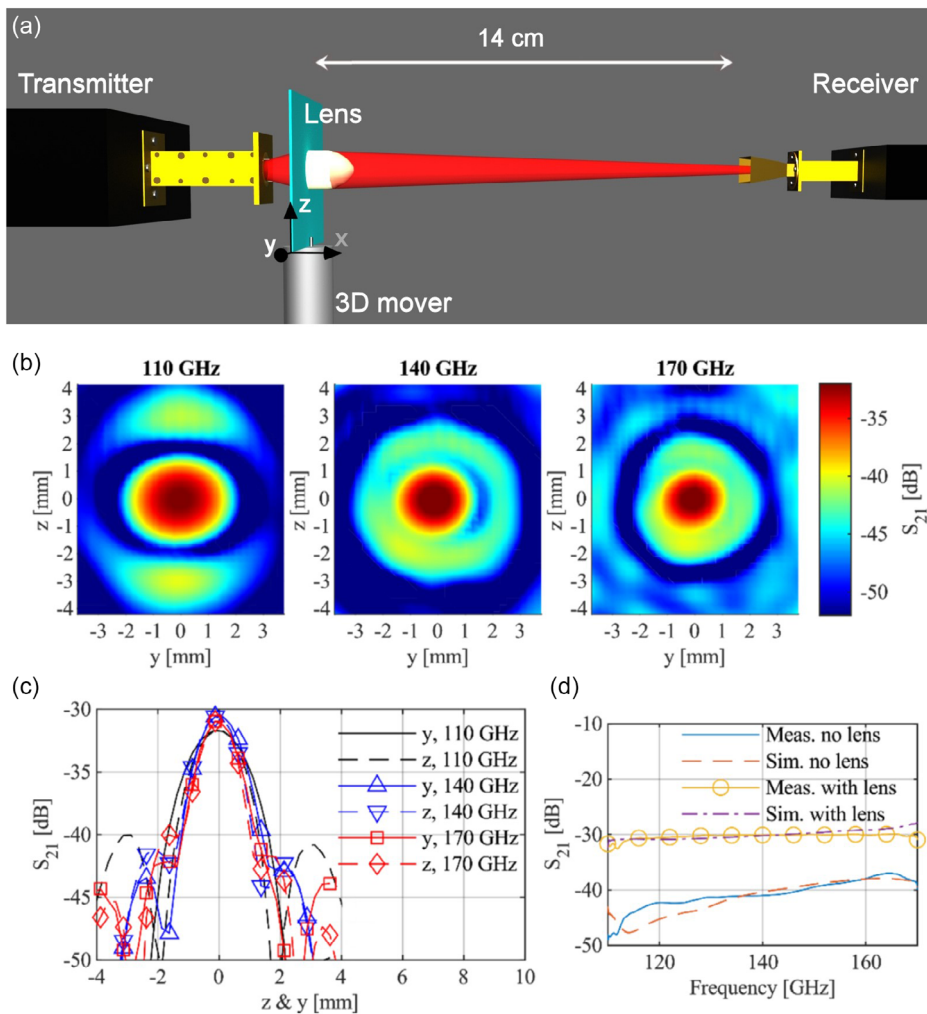


Figure 5. a) Schematic image of the measurement setup, b) lens deflected radiative near field measured by a horn antenna (14 cm transmitter–receiver distance), c) intensity distribution of the focal spot in y and z directions, and d) measured and simulated field strength with and without lens.

ring-shaped harmonics. Chromatic aberration (along with possible spherical aberration) as well as the frequency dependence of the loss factor can be reasons for the variation of the focal spot with the frequency. Furthermore, as the physical size of the lens is comparable to the wavelengths, even a small change of the frequency may result in different diffraction effects.^[23] It is also important to note that the measurement was conducted in the Fresnel region, thus the frequency dependence of the field distribution and intensities can be significant. The measured maximum of S_{21} had a mean variation of only 2.1 dB over the 110–170 GHz (Figure S2, Supporting Information) with a maximum increase of the intensity of the E-field of 17.2 dB measured at 110 GHz (Figure 5d and S1, Supporting Information).

5. Conclusion

Porous composites of SiO₂ nanoshells and PMMA having low dielectric permittivity ($\epsilon'_r = 1.5$ at 140 GHz) and loss factor ($\tan \delta = 4 \times 10^{-3}$ at 140 GHz) were synthesized and hot-pressed to form a bullet-shaped lens for focusing electromagnetic waves above 100 GHz. According to the measurements of scattering parameter, up to 17.2 dB increase of the field maybe achieved with the lens, indicating that the structure may find use in radiating near-field and in short range communication.^[24,25] The synthesis and postprocessing of the demonstrated porous composite is scalable and can be easily modified to tune not only the intrinsic dielectric material properties but also the size and geometry of lenses,^[26–28] making those suitable for various antenna^[29–32] and imaging^[33–35] applications near to THz frequencies.

Supporting Information

Supporting Information is available from the Wiley Online Library or from the author.

Acknowledgements

P.S.P. and M.K. contributed equally to this work. This work was supported by the 6G Flagship of the Academy of Finland under grant no. 318927.

Conflict of Interest

The authors declare no conflict of interest.

Data Availability Statement

The data that support the findings of this study are available from the corresponding author upon reasonable request.

Keywords

6G applications, low-loss dielectrics, low-permittivity materials, porous nanocomposites, templated sol-gel synthesis

Received: July 14, 2022
Revised: December 30, 2022
Published online: January 20, 2023

- [1] Z. Qadir, H. S. Munawar, N. Saeed, K. Le, *ICT Express* **2022**, <https://doi.org/10.1016/j.ict.2022.06.006>.
- [2] H. Viswanathan, P. E. Mogensen, *IEEE Access* **2020**, *8*, 57063.
- [3] A. L. Imoize, O. Adedeji, N. Tandiya, S. Shetty, *Sensors* **2021**, *21*, 57.
- [4] M. Giordani, M. Polese, M. Mezzavilla, S. Rangan, M. Zorzi, *IEEE Commun. Mag.* **2020**, *58*, 55.
- [5] M. H. Alsharif, A. H. Kelechi, M. A. Albreem, S. A. Chaudhry, M. S. Zia, S. Kim, *Symmetry* **2020**, *12*, 676.
- [6] J. C. Wiltse, in *Proc. SPIE - Int. Soc. Opt. Eng.*, Orlando, FL **2005**, Vol. 5790, p. 167.
- [7] H. D. Hristov, *Handbook of Antenna Technologies* (Eds: Z. Chen, D. Liu, H. Nakano, X. Qing, T. Zwick), Springer, Singapore **2016**.
- [8] C. A. Fernandes, E. B. Lima, J. R. Costa, in *Handbook of Antenna Technologies* (Eds: D. Liu, Z. N. Chen, H. Nakano, X. Qing, T. Zwick), Springer, Singapore **2016**, 1001–1064.
- [9] A. Ghavidel, S. Myllymäki, M. Kokkonen, N. Tervo, M. Nelo, H. Jantunen, *Prog. Electromagn. Res. Lett.* **2021**, *99*, 119.
- [10] R. T. Ako, A. Upadhyay, W. Withayachumnankul, M. Bhaskaran, S. Sriram, *Adv. Opt. Mater.* **2020**, *8*, 1900750.
- [11] M. K. Alkhafaji, H. A. Alhamadani, Y. I. A. Al-Yasir, A. L. Saleh, N. O. Parchin, R. A. Abd-Alhameed, *TELKOMNIKA* **2020**, *18*, 72.
- [12] W. Volksen, R. D. Miller, G. Dubois, *Chem. Rev.* **2010**, *110*, 56.
- [13] P. Xue, J. Feng, C. Xie, L. Wang, A. I. Tudi, E. V. Tikhonov, K. T. Butler, *J. Mater. Chem. C* **2021**, *9*, 15983.
- [14] T. Jiang, B. Zhu, S.-J. Ding, Z. Fanb, D. W. Zhang, *J. Mater. Chem. C* **2014**, *2*, 6502.
- [15] N. J. Trujillo, Q. Wu, K. K. Gleason, *Adv. Funct. Mater.* **2010**, *20*, 607.
- [16] B. Huang, K. Li, M. Peng, J. Cheng, *High Perform. Polym.* **2022**, *34*, 434.
- [17] Z. Hong, W. Dongyang, F. Yong, C. Hao, Y. Yusen, Y. Jiaojiao, J. Ligu, *Mater. Sci. Eng., B* **2016**, *203*, 13.
- [18] J. Jiao, L. Wang, P. Lv, P. Liu, Y. Cai, *Mater. Lett.* **2013**, *109*, 158.
- [19] Y. Wang, Z. Yang, H. Wang, E. Li, Y. Yuan, *J. Mater. Sci. Mater. Electron* **2022**, *33*, 4550.
- [20] T. Chang, X. Zhang, X. Zhang, H.-L. Cui, *Appl. Opt.* **2017**, *56*, 3287.
- [21] P. S. Pálvölgyi, M. Nelo, O. Pitkänen, J. Peräntie, H. Liimatainen, S. Myllymäki, H. Jantunen, K. Kordas, *Nanotechnology* **2020**, *31*, 435203.
- [22] V. A. Markel, *J. Opt. Soc. Am. A* **2016**, *33*, 1244.
- [23] J. Thornton, K.-C. Huang, *Modern Lens Antennas for Communications Engineering*, Wiley-IEEE Press, Hoboken, NJ **2013**.
- [24] K. Guan, H. Yi, D. He, B. Ai, Z. Zhong, *China Commun.* **2021**, *18*, 18.
- [25] D. He, K. Guan, A. Fricke, B. Ai, R. He, Z. Zhong, A. Kasamatsu, I. Hosako, T. Kurner, *IEEE Trans. Terahertz Sci. Tech.* **2017**, *7*, 502.
- [26] J. Volakis, *Antenna Engineering Handbook*, 4th ed., McGraw-Hill, New York **2007**.
- [27] Y. He, Y. Chen, L. Zhang, S.-W. Wong, Z. N. Chen, *China Commun.* **2020**, *17*, 124.
- [28] C. A. Fernandes, E. B. Lima, J. R. Costa, *Handbook of Antenna Technologies* (Eds: Z. N. Chen, D. Liu, H. Nakano, X. Qing, T. Zwick), Springer, Singapore **2016**, p. 1001.
- [29] B. Ahmed, I. Saleem, H. Zahra, H. Khurshid, S. M. Abbas, *Int. J. Future Gener. Commun. Netw.* **2012**, *5*, 113.
- [30] J.-C. Y. Thierry, V. Ungvichian, J. A. Barbosa, *J. Comput.* **2009**, *4*, 610.
- [31] J. W. Salman, M. M. Ameen, S. O. Hassan, *J. Eng. Dev.* **2006**, *10*, 1.
- [32] P. Puttaswamy, P. Srivatsa, K. Murthy, B. Thomas, *Int. J. Appl. Sci. Eng. Res.* **2014**, *3*, 1102.

- [33] D. M. Mittleman, R. H. Jacobsen, M. C. Nuss, *IEEE J. Sel. Top. Quantum Electron.* **1996**, 2, 679.
- [34] A. Y. Pawar, D. D. Sonawane, K. B. Erande, D. V. Derle, *Drug Invent. Today* **2013**, 5, 157.
- [35] P. Hillger, J. Grzyb, R. Jain, U. R. Pfeiffer, *IEEE Trans. Terahertz Sci. Technol.* **2019**, 9, 1.
- [36] K. Konstantinidis, A. P. Feresidis, C. C. Constantinou, E. Hoare, M. Gashinova, M. J. Lancaster, P. Gardner, *IEEE Trans. Terahertz Sci. Tech.* **2017**, 7, 572.
- [37] N. Chudpooti, N. Duangrit, P. Akkaraekthalin, I. D. Robertson, N. Somjit, *IEEE Access* **2019**, 7, 12283.
- [38] E. Lacombe, F. Giansello, A. Bisognin, C. Luxey, A. Bisognin, D. Titz, H. Gulan, T. Zwick, J. Costa, C. A. Fernandes, in *IEEE Int. Symp. Antennas Propag. USNC/URSI Nat. Radio Sci. Meeting*, San Diego, CA **2017**, p. 5.
- [39] N. Duangrit, B. Hong, A. D. Burnett, P. Akkaraekthalin, I. D. Robertson, N. Somjit, *IEEE Access* **2019**, 7, 12339.
- [40] A. Jouade, M. Himdi, O. Lafond, *IEEE Trans. Antennas Propag.* **2017**, 65, 5776.